Analytica Chimica Acta 1121 (2020) 17–25

Contents lists available at ScienceDirect

Analytica Chimica Acta

journal homepage: www.elsevier.com/locate/aca

Highly sensitive electrochemical detection of circulating tumor DNA in human blood based on urchin-like gold nanocrystal-multiple graphene aerogel and target DNA-induced recycling double amplification strategy

Peng Yuanfeng [a], Li Ruiyi [b], Sun Xiulan [c], Wang Guangli [a], Li Zaijun [a, *]

[a] The Key Laboratory of Synthetic and Biological Colloids, Ministry of Education, School of Chemical and Material Engineering, Jiangnan University, Wuxi, 214122, China
[b] School of Pharmaceutical Sciences, Jiangnan University, Wuxi, 214122, China
[c] School of Food Science and Technology, Jiangnan University, Wuxi, 214122, China

HIGHLIGHTS

- We report control synthesis of gold nanocrystals via reduction of $HAuCl_4$ with ascorbic acid.
- The gold nanocrystals shows an urchin-like structure with more exposed high-index facets.
- Unique structure produces high chemical activity and catalytic activity of gold nanocrystals.
- Proposed method has ultrahigh sensitivity, specificity and stability for detection of ctDNA.
- The synthesis can use for synthesis of other metal nanocrystals with high catalytic activity.

GRAPHICAL ABSTRACT

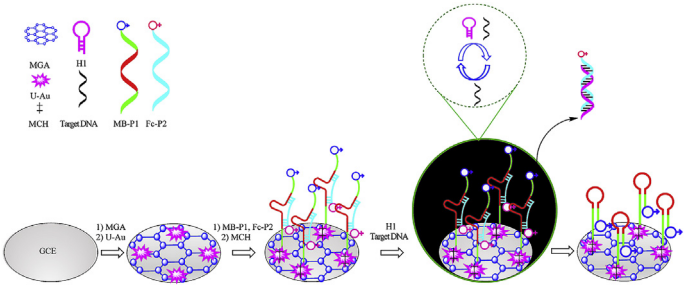

ARTICLE INFO

Article history:
Received 10 April 2020
Received in revised form
26 April 2020
Accepted 30 April 2020
Available online 5 May 2020

Keywords:
Tumor diagnosis
Voltammetry
Enzyme-free signal amplification
Shape-controlled synthesis

ABSTRACT

Detection of circulating tumor DNA (ctDNA) is important approach to risk stratification and treatment response monitoring of cancer patients, but current method lacks of enough sensitivity and repeatability. The paper repors shape-controlled synthesis of gold nanocrystals via reduction of $HAuCl_4$ with ascorbic acid. The synergy of CTAC, KBr, KI and L-glutathione creates urchin-like gold nanocrystals (U–Au) with more exposed high-index facets. Preparation of electrochemical sensing platform for ctDNA involves modification of U–Au-multiple graphene aerogel for target DNA-induced recycle amplification. DNA probe 1 (P1) with methylene blue (MB) hybridizes with DNA probe 2 with ferrocene (Fc) to form duplex DNA, which was attached to U–Au through Au–S bond. The ctDNA hybridizes with hairpin DNA 1 to open hairpin structure, triggering target DNA-induced recycle. Utilization of target DNA-induced recycling allows one target DNA to approach many MB probes to electrode surface and to leave many Fc probes from electrode surface, promoting significant signal amplification. The detection signal is enhanced by catalyzed redox of Fc and MB. Electrochemical response increases with ctDNA concentration

* Corresponding author.
E-mail address: zaijunli@jiangnan.edu.cn (L. Zaijun).

https://doi.org/10.1016/j.aca.2020.04.077

from 0.1 to 1 × 10^6 fM with detection limit of 0.033 fM. The biosensor provides ultrahigh sensitivity, specificity and stability and was successfully applied in detection of ctDNA in human blood.

1. Introduction

Malignant tumor has become the leading cause of death in contemporary world. According to the statistics presented by the World Health Organization (WHO), there were 8.8 million cancer deaths worldwide in 2015 [1]. The number of cancer patients are expected to exceed 24.6 million by 2030 [2]. The importance of early diagnosis of cancer become more and more prominent with increasing attention to health. Circulating tumor DNA (ctDNA), as a potential tumor biomarker, is released by the tumor or circulating tumor cells into the patient's blood in the initial form of cancer development [3]. Cancer patients have a higher ctDNA level compared to healthy individual. The mutations in the KRAS gene are one of the most commonly used molecular mutations in ctDNA detection, which can be detected in healthy controls within two years before the tumor diagnosis [4]. The development of rapid and reliable methods for quantitative detection of ctDNA is of significance for clinical diagnosis, prognosis monitoring and drug resistance testing of tumors.

The main analytical techniques for detection of ctDNA are polymerase chain reaction (PCR) [5], DNA sequencing [6], surface enhanced aman spectroscopy (SERS) [7], localized surface plasmon resonance (LSPR) [8] and DNA clutch probes (DCPs) [9]. PCR is tedious in steps and easily disturbed by biological environment, resulting in false positive/negative signals. DNA sequencing has a better sensitivity and specificity compared to PCR. Unfortunately, it requires expensive equipment and long analysis time [10]. This greatly limits many applications of DNA sequencing in clinical diagnosis. Recently, electrochemical biosensor attracted more attention due to its high sensitivity, good specificity and real-time and economic efficiency operation. To improve the analytical performance, numerous nanomaterials have been investigated as the electrochemical sensing materials for the construction of electrochemical biosensors [11–13], such as Fe_3O_4/N-trimethyl chitosan/gold composite [14], doxorubicin@tetrahedron-functionalized gold nanoparticles [15], graphene-carboxymethylcellulose [16], gold nanoparticles/polyethylene glycol film [17], Si_3N_4/Au/Pd [9] and gold nanoparticles/lead phosphate apoferritin [18]. Due to high biocompatibility, electronic conductivity and catalytic activity, gold nanomaterials become the most commonly used electrochemical sensing material.

Shape-controlled synthesis is an effective way to improve the catalytic activity of gold nanocrystals [19]. Zhang and co-workers [20] reported that the precursor formed by mixing urea with $HAuCl_4$ was calcined and reduced to produce porous gold nanoparticles under the aerobic condition. The resulting porous gold displays more than 6-fold catalytic activity of common gold nanoparticles. Liu and co-workers synthesized a kind of hollow Au–Ag nanoalloy by electrochemical method, which shows a high SERS catalytic activity towards crystal violet [21]. However, small or hollow gold nanoparticles often offer a relatively low electronic conductivity. Constructing core-shell structures or nanoclusters can improve the conductivity of gold nanoparticles. Our group reported the synthesis of palladium@gold nanoalloy-graphene multiple aerogels composite [22]. In the composite, palladium nanocube core enhances the electronic conductivity and gold nanoparticle shell improves the catalytic activity. Recenly, many researches demonstrated that the high-index facet of gold nanocrystals has a better catalytic activity compared to the low-index facet of gold nanocrystals [23,24]. Unfortunately, the high-index facets are rapidly closed by the low-index facets due to their low growth rate. Although a great progress has been made, the shape-controlled synthesis of gold nanocrystals with more exposed high-index facets is still a great challenge.

In the study, we report the shape-controlled synthesis of gold nanocrystals via reduction of $HAuCl_4$ with ascorbic acid. The result shows that the synergy of CTAC, KBr, KI and L-glutathione as the shape control agents creates urchin-like gold nanocrystals (U–Au) with multistage spiny structures and more exposed high-index facets. The electrochemical biosensor based on U–Au-multiple graphene aerogel and target DNA-induced recycling double amplification displays the enhanced sensitivity, specificity and repeativity for detection of ctDNA.

2. Experimental

2.1. Materials and reagents

Multiple graphene aerogel (MGA) was prepared by using the reported method [25]. All nucleic acids in Table 1 were made and purified by Sangon Biotech. Co., Ltd (Shanghai, China). The concentration of oligonucleotides was determined by measuring absorption at 260 nm. The DNA stock solution was prepared in the Tris/Mg/K buffer containing 20 mM Tris-HCl, 1 mM $MgCl_2$, 1 mM $CaCl_2$ and 5 mM KCl at pH 7.4 and stored at −20 °C for further use.

2.2. U–Au synthesis

U–Au was synthesized by reduction of $HAuCl_4$ with ascorbic acid. In a typical procedure, an ascorbic acid aqueous solution (0.45 mL, 100 mM) was rapidly injected into 5 mL of the mixture of $HAuCl_4$ (0.4 mM), CTAC (0.16 mM), KBr (10.0 μM), KI (1.0 μM) and L-glutathione (5.0 μM) under stirring. The mixture was incubated at the ambient temperature for 30 min. It was treated by centrifugation at 6000 rpm for 2 min and washing with ultrapure water for three times. The collected U–Au product was dispersed again in ultrapure water and stored at 4 °C for further use.

2.3. Electrode modification

The U–Au solution (0.5 mL, 1.0 mg mL^{-1}) and MGA dispersion (0.5 mL, 1.0 mg mL^{-1}) were dispersed in 1 mL of 5% chitosan aqueous solution with the help of ultrasound. Firstly, its 5 μL was dropped on the surface of glassy carbon electrode (GCE, 1 mm in diameter) pre-treated by using a classical procedure [26] and dried at 4 °C to obtain U–Au-MGA/GCE. Then, the MB-P1 solution (100 μL, 10 μM) was mixed with an equal volume of TCEP solution (1 mM) and incubated in air bath shaker for 1 h to activate the −SH groups. The 10 μL of the mixture of MB-P1 (5 μM) with Fc-P2 (5 μM) was dropped on the surface of U–Au/MGA/GCE and incubated at 37 °C for 2 h. Finally, 5 μL of the MCH solution (1 mM) was dropped on the electrode surface and incubated for 60 min to block the unmodified sites on the U–Au surface. The resulting MCH/MB-P1-Fc-P2/U–Au-MGA/GCE was rinsed with the PBS buffer for several

Table 1
The base sequences of oligonucleotides used in the work.

Oligonucleotides	Base sequences (5′-3′)
Target DNA (ctDNA)	TTGTGGTAGTTGGAGCTGATGGCGTAGGCAA
Hairpin DNA 1 (H1)	AGCTCCAACTACCACAAGCAGACGTACCGTGGTAGTT
DNA probe 1 modified with ferrocene (Fc-P1)	AACTACCACGGTACGTCTGCTTGTGGTAGTT-Fc
DNA probe 2 modified with Methylene blue and thiol (MB-P2)	SH-$(CH_2)_6$-TGGCAGACGGGACGACCCCCCTCGTCCGGTGGTAGTG-MB
Wide type	TTGTGGTAGTTGGAGCTGGTGGCGTAGGCAA

times, dried at room temperature and stored at 4 °C for further use.

2.4. Electrochemical detection of ctDNA

The target DNA (ctDNA) solution with different concentration or sampe solution (10 μL) was mixed with the annealed H1 (10 μL, 5 μM). Its 10 μL was dropped onto the surface of MCH/MB-P1-Fc-P2/U–Au-MGA/GCE, incubated at room temperature for 1 h and washed with the PBS (pH 7.4) in sequence. The electrode was immersed in the PBS buffer for the DPV measurement.

2.5. Extraction of ctDNA

All participants provided the written informed consent for the collection of samples for the research study protocol, which was approved by the Research Ethics Committee of Jiangnan University. The blood samples used in this work were provided by the Affiliated Hospital of Jiangnan University. The sample was centrifuged to obtain plasma, which was used for the extraction of ctDNA by using the QIAamp DNA Blood Mini Kit(Qiagen, Germany). In a typical procedure, 200 μL of the plasma was added to a microcentrifuge tube containing 20 μL of QIAGEN protease, mixed with 200 μL of lysis buffer by pulsed vortex for 15 s to obtain a homogeneous solution, followed by incubation at 56 °C for 10 min, and the microcentrifuge tube was briefly centrifuged to remove the inner droplets. Subsequently, 200 μL of the ethanol (96–100%) was added, mixed by vortex for 15 s, and then centrifuged at 8000 rpm for 1 min using a rotating column for DNA extraction, followed by 500 μL of two types of the washing buffer for centrifugation for 1 min to enrich the required DNA. Finally, 200 μL distilled water was added, incubated at room temperature for 1 min, and centrifuged at 8000 rpm for 5 min to obtain enriched DNA, which was stored at −20 °C.

3. Results and discussion

3.1. U–Au synthesis

U–Au was synthesized by reduction of $HAuCl_4$ with ascorbic acid. In the synthesis, CTAC, KBr, KI and L-glutathione were used as the shape control agents for the construction of gold nanocrystals with more exposed high-index facets. CTAC, a classical cationic surfactant, was designed as a soft template. The template provides a micron-sized space for the reduction of Au^{3+} into Au^0 and the crystal growth. The space alows the formation of large gold nancrystals [27]. Furthermore, CTA^+ and Cl^- in the CTAC can be effectively adsorbed on the crystal faces of gold nanocrystals. Because the adsorption capacity of CTA^+ and Cl^- on the different crystal face results in a different growth rate for different crystal face, CTAC has been widely applied in the synthesis of gold nanocrystals with different morphologies [28]. KBr and KI were used for improving morphology uniformity of gold nanocrystals. Different halogen ion has a different adsorption behavior and chemical properties. This difference directly reflects in the regulation of morphology of gold nanocrystals. Hence, the cooperation of Cl^-, Br^- and I^- may achieve an effective control of morphology of gold nanocrystals [29,30]. In addition, the introduction of KBr and KI was also used to accelerate the reduction of Au^{3+} in the synthesis. Br^- and I^- can react with Au^{3+} to form stable $AuBr_4^-$ and AuI_4^-. The formation of these complexes reduces the reduction potential of Au^{3+}, which results in an accelerated reduction of Au^{3+} and crystal growth rates. L-glutathione was used to improve the exposure of high-index crystal facets of gold nanocrystals. L-glutathione is a chiral molecule with sulfhydryl group. The enantioselective interaction on the interfaces caused by L-glutathione leads to an asymmetric crystal growth, which improves the exposure of high-index facets [31].

In the synthesis of U–Au, the dosage of KBr, KI and L-glutathione is very small but the effects are very great. To simplify the operation and improve the repeatability of batch production, $HAuCl_4$, CTAC, KBr, KI and L-glutathione were firstly dissolved in ultrapure water at a predetermined molar ratio to form a stocking solution. Then, U–Au was prepared by one-step simaple injection of the ascorbic acid solution into the above stocking solution. Such a synthesis strategy displays simple operation, high efficiency and good repeatability of batch production.

The as-synthesized U–Au was characterized by SEM, TEM and XRD. Fig. 1 shows the U–Au processes urchin-like nanostructures with multilevel spiny structures, large size of about 400 nm and more exposed high-index facets, which is mainly due to the synergy of CTAC, KBr, KI and L-glutathione as the shape control agents. Small and dense secondary spikes make the U–Au has large specific surface area and more exposed high-index facets. The former contributes to increase the contact area between electrolyte and redox. The latter brings a better catalytic activity. The integration of primary and secondary spikes achieves to high catalytic acitivity of U–Au [32]. There is one crystal plane spacing of 0.235 nm on the high-resolution TEM (HRTEM) image, corresponding to the (200) crystal plane of gold nanocrystals. There are eight XRD characteristic diffraction peaks at 38.17°, 44.47°, 64.65°, 77.64°, 81.80°, 98.13°, 110.91° and 115.33° on the XRD pattern. These peaks are correspond to the (111), (200), (200), (220), (311), (222), (400), (311) and (420) crystal facets of gold nanocrystals. The XRD pattern are exactly matched with that of FCC gold (JCPDS 4–0784), indicating that our synthesis achieves the synthesis of FCC gold nanocrystals. Relative to the Au-0 prepared by using the sample procedure but no addition of CTAC and L-glutathione (Fig. s1), the U–Au displays an enhanced XRD diffraction intensity of high-index facets such as the (331) and (420) facets. This proves that the introduction of CTAC and glutathione can improve the exposure of high-index facets of gold nanocrystals, leading to an improved catalytic activity. To verify the suggest, the SERS performance of rhodamine 6G on the U–Au and Au-0 substrates were investigated. Fig. 1F shows that different substrate material produces different SERS performance. The intensity on the U–Au at 809 cm^{-1} is more than 24 fold than that on the Au-0, representing ultra strong surface plasmon resonance. This is attributed to the multilevel spiny urchin-like nanostructures of U–Au. This brings an improved catalytic activity and results in more sensitive electrochemical response towards ctDNA.

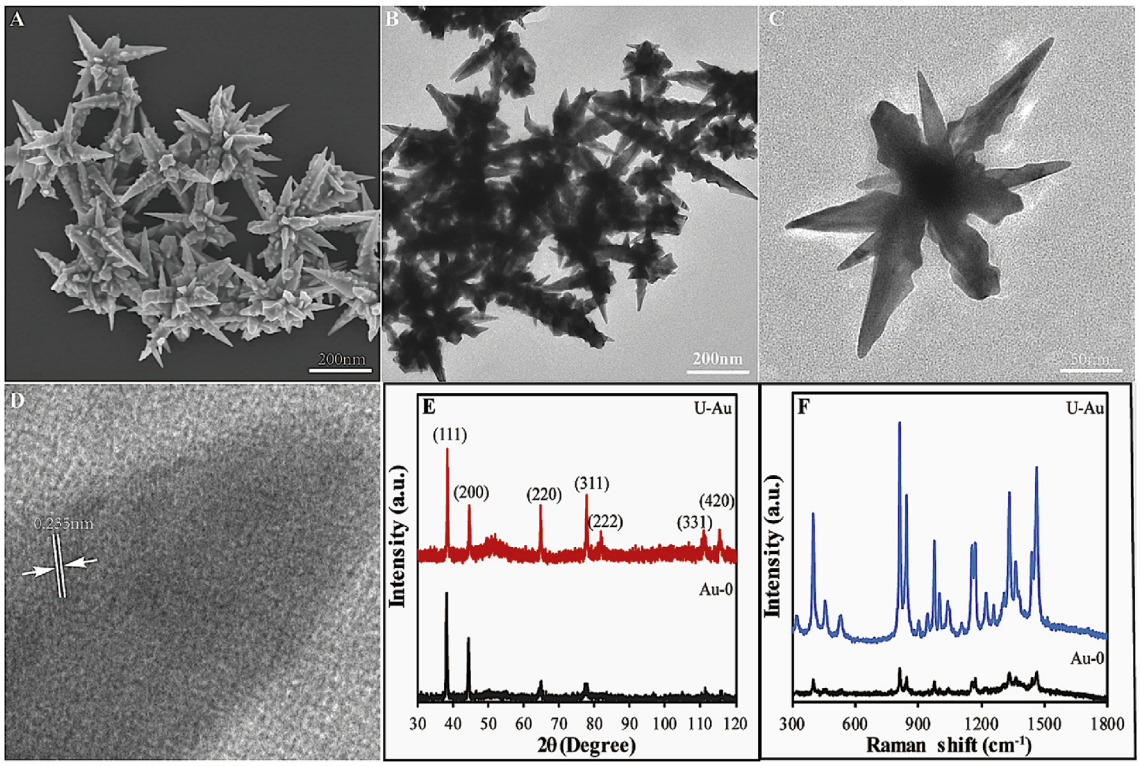

Fig. 1. The SEM (A), TEM (B), enlarged TEM (C), HRTEM images (D), XRD patterns (E) and Raman spectrum (F) of U–Au.

3.2. Sensing principle

The intergation of U–Au and MGA further improves the electron transfer and electrolyte transport between electrode and electrolyte. Herein, the U–Au-MGA composite was used for the construction of electrochemical sensing platform for ctDNA coupled with target DNA-induced recycling ampilification (Fig. 2). Firstly, the U–Au-MGA was modified on the surface of GCE. The composite greatly improves the electron transfer and eletrolyte transport during the electrode reaction. More importantly, the composite acts as the catalyst, which accelerates the redox of Fc and MB on the electrode surface. Next, the MB-P1 hybridizes with Fc-P2 to form deplex DNA. At the same time, the MB-P1 was immobilized on the surface of U–Au via Au–S bond. At this state, the MB is far away from the electrode interface, resulting in a weak DPV current of MB (I_{MB}). The Fc is close to the electrode interface, leading to a strong DPV current of Fc (I_{fc}). In the presence of target DNA, ctDNA is complementary paired with H1 on the electrode surface through base pairing to open hairpin structure of H1. The opened H1 and Fc-P1 in the deplex DNA continue to complement each other, releasing one target DNA and starting next DNA recycle. In the process, the MB-P1 is dissociated from the deplex DNA and folds into the hairpin structure. At this state, the Fc probe was released from the electrode surface and the MB probe was close to the electrode interface, causing a decrease in I_{Fc} and an increase in I_{MB}. Through the target DNA-induced recycling reaction, one target DNA

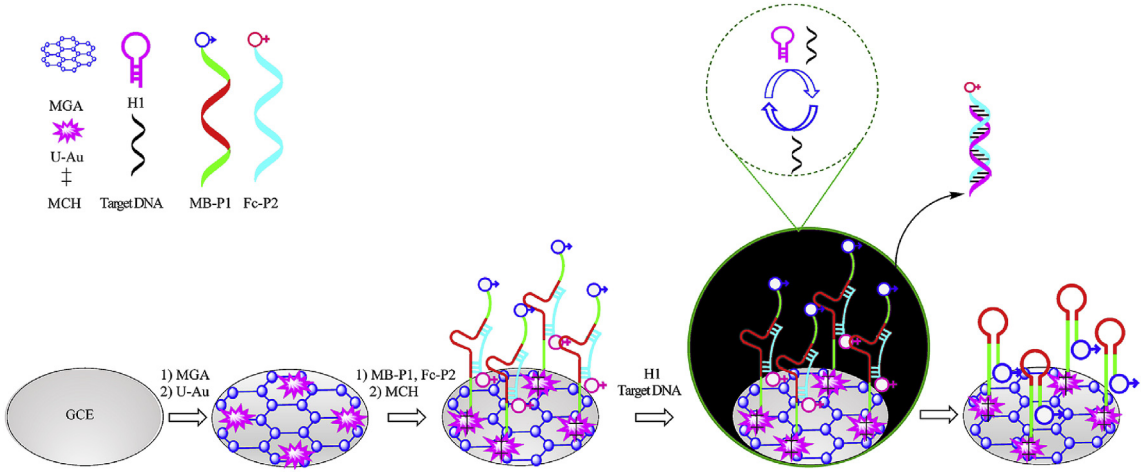

Fig. 2. The scheme for construction of electrochemical sensing platform for ctDNA.

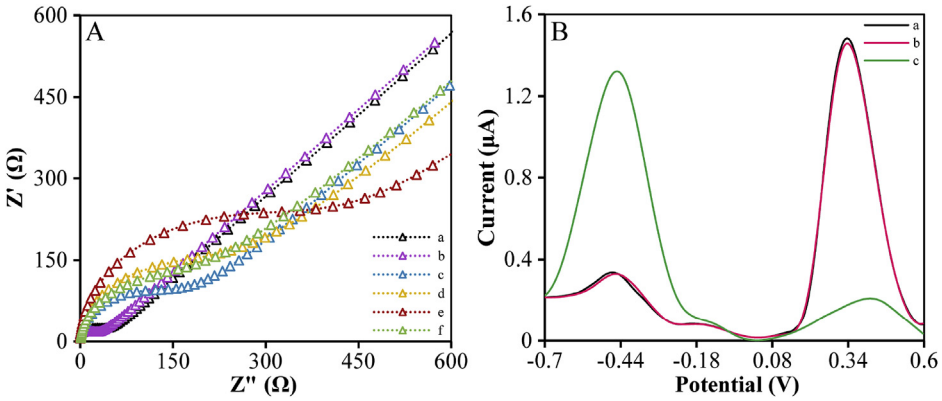

Fig. 3. A: The EIS curves in a 5.0 mM $Fe(CN)_6^{4-}$ solution of the bare GCE (a), U–Au-MGA/GCE (b), MB-P1-Fc-P2/U–Au-MGA/GCE (c), MCH/MB-P1-Fc-P2/U–Au-MGA/GCE before (d) and after incubated in the H1 solution for 1 h in the absence (e) and the presence of target DNA (f). B: The DPV curves in the PBS of pH 7.4 of MCH/MB-P1-Fc-P2/U–Au-MGA/GCE before (a) and after incubated in the H1 solution in the absence (b) and the presence (c) of target DNA for 1 h.

molecule can cause many MB probes to approach the electrode surface and many Fc probes to stay away from the electrode surface. This produces a significant signal amplification. The detection signal will be further enhanced by the in stiu catalysis of U–Au-MGA to Fc and MB, due to excellent catalytic activity of U–Au. Therefore, the as-proposed sensing platform can be used for the electrochemical detection of ctDNA with high sensitively and specifity by analyzing the ratio of peak current signals of two redox probes before and after adding target ctDNA.

To test the feasibility of the detecting ctDNA, the EIS behavior of different electrodes was studied in 1 mM Fe $(CN)_6^{4-}$. Fig. 3A shows the U–Au-MGA/GCE has a lower charge transfer impedance (R_{ct}) compared to the bare GCE. This is due to high electron/ion conductivity and catalytic activity of U–Au-MGA. The R_{ct} value increases after the MB-P1 hybridizes with Fc-P2 on the electrode surface. The hybridization produces the deplex DNA with poor electronic conductivity, which partially block the channels for electron transfer/elelctrolyte between electrode and electrolyte. Fourthermore, there is strong repulsion force between negatively charged $Fe(CN)_6^{4-}$ and DNA phosphate skeleton. The fators leads to an increased R_{ct} value. The R_{ct} value further increases after MCH was immoblized on the electrode surface, owing to more blocking of the channels for the electron transfer between electrode and electrolyte. The R_{ct} value remains stable before and after incubated in a H1 solution without the target DNA. In the absence of target DNA, the incubation cannot trigger the target DNA-induced recycling. As the structure of Fc-P1-MB-P2 was not changed, no obvious change in the R_{ct} value occurs in the incubation process. However, the incubation in the presence of target DNA causes a significant reduce in R_{ct} value. In the presence of target DNA, the hybridization of target DNA hybridizes with H1 opens the hairpin structure of H1. The opened H1 binds with the Fc-P1-MB-P2 to trigger the target DNA-induced recycle. Through the target ctDNA-induced DNA cycling reaction, one target DNA can cause many Fc probes to leave the electrode and many MB probes to approach the electrode surface, decreasing the R_{ct} value. The R_{ct} value is further reduced by the in situ catalysis of U–Au-MGA towards the redox of MB. This improves the sensitivity for electrochemical detection of ctDNA.

3.3. Electrochemical response

To examine the electrochemical response towards ctDNA, the DPV behavior of MCH/MB-P1-Fc-P2/U–Au-MGA/GCE incubated in the H1 solution in the presence of target DNA was investigated in the PBS at pH 7.4. Fig. 3B shows that after incubated in the H1 without target DNA the DPV peak current in the negative potential region, correspinding to the Fc probe, is weak and while the peak current in the positive potential region, corresponding to the MB probe, is strong. The DPV curve is approximately the same as the DPV curve before incubated. As the target DNA-induced recycling can not be triggered in the absence of target DNA, no change in the structure of MB-P1-Fc-P2/U–Au-MGA occurs in the incubation process. Thus, its DPV response remains stable. However, in the presence of target DNA, the incubation results in an increased DPV response of Fc probe and a decreased DPV response of MB probe. This is because the presence of target DNA brings many MB probes to approach the electrode surface, indicating an increased peak current of MB, and many Fc probes to lease from the electrode surface, indicating decreased peak current of Fc. The above results confirm that only ctDNA can cause a sensitive DPV response.

3.4. Condition optimization

To optimize the detection conditions, the effect of H1 concentration and incubation time on the DPV response (I_{MB}/I_{Fc}) were investigated in the PBS. Fig. 4A presents the relationship cure of the I_{MB}/I_{Fc} value with the H1 concentration. When the H1 concentration is less than 5 μM, the I_{MB}/I_{Fc} value increases with increasing H1 concentration. The value reaches the maximum when the H1 concentration is at 5 μM H1 and then tends to be stable with increasing H1 concentration. In a low H1 conentration, the MB-P1-Fc-P2 structures cannot be completely decomposed to release free MB-P1 due to a low target DNA-induced recycling reaction rate. The number of hairpin MB-P1 probes increases with increasing H1 concentration, leading to an increased peak current of MB and a reduced peak current of the Fc probe. Hence, a bigger H1 concentration results in a higher I_{MB}/I_{Fc} value. In the presence of 5 μM H1, all MB-P1-Fc-P2 structures can be decomposed by the target DNA-induced recycling reaction to produce the hairpin MB-P1 on the electrode surface, due to a fast reaction rate. This brings the maximum peak current of MB probe and the minimum peak current of Fc probe, indicating the maximum I_{MB}/I_{Fc} value. However, the number of hairpin MB-P1 probes no longer increases significantly with increasing H1 concentration. As a result, there is no obvious change in the I_{MB}/I_{Fc} value. Fig. 4B presents the relationship curve of the I_{MB}/I_{Fc} value with the incubation time. When the time was less than 60 min, the peak current increases with the prolongation of incubation time. This is because the number of target-induced DNA cycles increases with increasing the incubation time. This results in more MB probes to approach the electrode

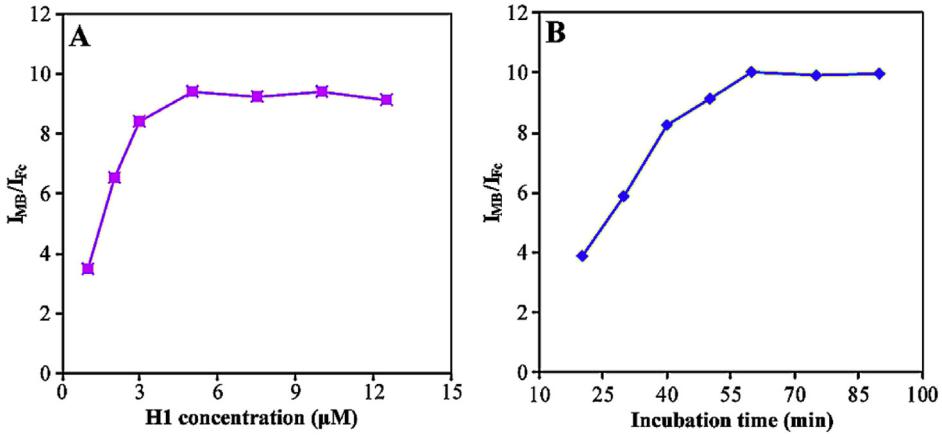

Fig. 4. The effects of H1 concentration (A) and incubation time (B) on the I_{MB}/I_{Fc} value caused by target DNA.

surface and more Fc probes to remove from the electrode surface, producing a higher I_{MB}/I_{Fc} value. When the incubation time was fixed for 60 min, the targe DNA-induced recycling reaction is close to the equilibrium. The number of harpin MB-P1 probes reach the maximum, leading to the maximum the I_{MB}/I_{Fc} value. Continue to increase the incubation time, this number will not increase significantly. Thus, the I_{MB}/I_{Fc} value remains stable with increasing the incubation time. To obtain high sensitivity and save analysis time, the H1 concentration of 5 μM and incubation time of 60 min were adopted for the electrochemical detection of ctDNA.

3.5. Analytical characteristics

Fig. 5A shows the DPV curves of MCH/MB-P1-Fc-P2/U–Au-MGA/GCE in the PBS buffer of pH 7.4 after incubated in the H1 solution containing different concentration of ctDNA for 60 min. Under the optimized conditions, the DPV current of MB increases with increasing the ctDNA concentration. This is because the target DNA-induced recycling has a faster speed in the presence of a higher ctDNA concentration compared to that in a lower ctDNA concentration. When the incubation time is fixed at 60 min, more MB probes are close to the electrode surface and many Fc probes was released from the electrode surface with increasing ctDNA concentration, causing an enhanced I_{MB} value and a decreased I_{Fc} value, indicating increased I_{MB}/I_{Fc} value. Further, the relationship curve of the logarithm of I_{MB}/I_{Fc} with the logarithm of ctDNA concentration. There is a good linear relationship between the logarithm of I_{MB}/I_{Fc} and the logarithm of ctDNA concentration in the range of 0.1–1.0 × 10^6 fM. The linear regression equation is: $Log(-I_{MB}/I_{Fc}) = 0.242 \times Log(C_{ctDNA}, fM)+0.268$, with the correlation coefficient (R^2) of 0.998. The detection limit (LOD) is 0.033 fM for the detection of ctDNA (N/S = 3). The result shows that the as-proposed biosensor has a better sensitivity compared to other methods for electrochemical detection of ctDNA in Table 2. Sixty duplicate measurements show a relative standard deviation of 2.5%, verifying high repeatability. The stability of MCH/MB-P1-Fc-P2/U–Au-MGA/GCE was examined by storing it at 4 °C for 30 days. Then, the I_{MB}/I_{Fc} value caused by 10 fM ctDNA was measured. The result shows that the I_{MB}/I_{Fc} value remains at about 99.6% after this time, indicating good stability.

To evaluate the effect of U–Au on the sensitivity in the as-proposed electrochemical sensing platform, another gold nanomaterial (Au-0) was prepared by the same procedure as the synthesis of U–Au without CTAC and L-glutathione and used for the biosensor preparation for detection of ctDNA. As shown in Fig. 5C and D, the biosensor with U–Au or Au-0 can produce a high DPV current response towards ctDNA. However, the sensitivity of biosensor with U–Au is better than that of the biosensor with Au-0 for the same ctDNA concentration. The change in the I_{MB}/I_{Fc} vaue of biosensor with U–Au is more than that of biosensor with Au-0, verifying that the use of U–Au as the sensing material causes a significant enhancement of the detection signal. This enhancement is mainly attributed to high catalytic activity of U–Au. Different from spherical Au-0, U–Au has an urchin-like architecture with multilevel spiny structures and more exposed high-index facets. The unique structure chieves to high catalytic activity. As a result, in situ catalysis of U–Au towards redox of MB and Fc on the electrode surface causes sensitive DPV response. This further enhances the sensitivity for detection of ctDNA.

To examine the specificity of as-proposed biosensor for the

Table 2
Comparison of analytical characteristics of different electrochemical biosensors for detection of ctDNA.

Sensing material	Detection technique	Target specie	Linear range	Detection limit	Ref.
DNA clutch probes (DCPs)/nanostructured microelectrodes equipped with PNA probe clamps	Differential pulse voltammetry	ctDNA		1 fg μL^{-1}	[9]
AuNP/PNA probes	LSPR spectra	PIK3CA		50 fM	[8]
Doxorubicin@tetrahedron-Au	Differential pulse voltammetry	KRAS	1fM-10nM	0.29 fM	[15]
DNA three-way junction	Square wave voltammetry	ctDNA	10^{-15} -10^{-11}M	4.1 × 10^{-16}M	[33]
Nickel(II) phenanthroline complex	Differential pulse voltammetric	ctDNA	1 −15 μg mL^{-1}	0.18 μg mL^{-1}	[34]
Urchins-like gold nanocrystal/GO	Differential pulse voltammetric	KRAS	0.1−10^6fM	0.031 fM	This work

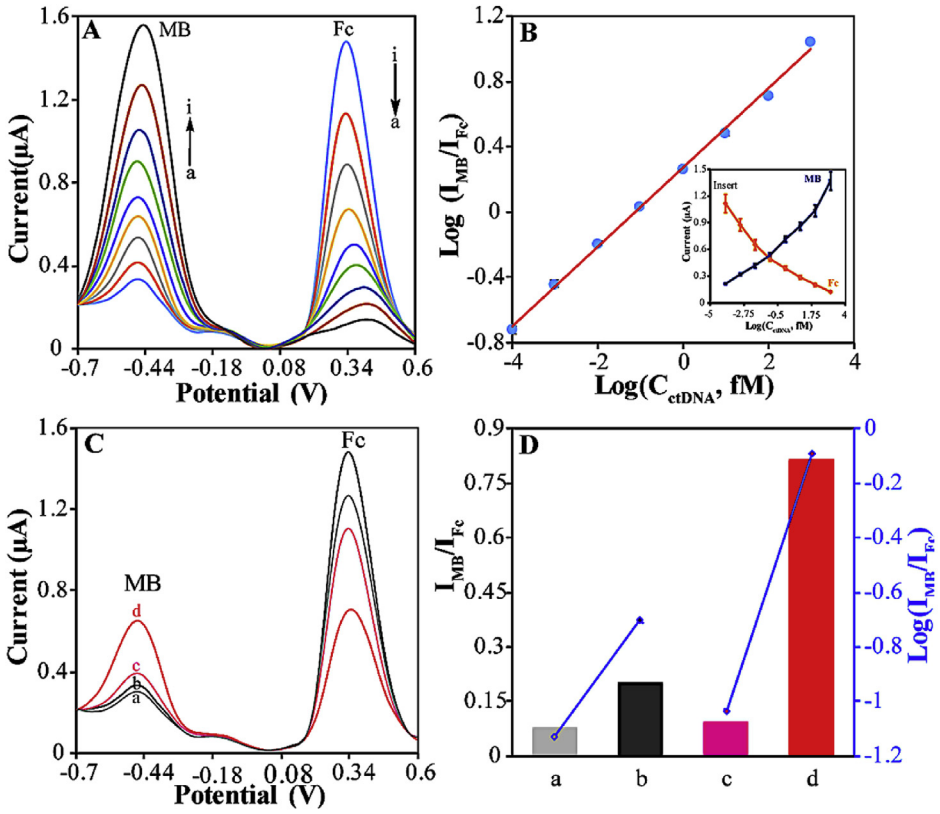

Fig. 5. The DPV curves (A) of MCH/MB-P1/Fc-P2/U–Au-MGA/GCE in the PBS of pH 7.4 after incubated in the H1 solution containing 0.0, 0.1, 1.0, 10.0, 100.0, 1000.0, 10000.0, 100000.0 and 1000000 fM ctDNA (from a to i), the relationship curve (B) of the logarithm of DPV peak current ratio (I_{MB}/I_{Fc}) with the logarithm of ctDNA concentration, the DPV curves (C) and the I_{MB}/I_{Fc} values (D) of MCH/MB-P1/Fc-P2/Au-0-MGA/GCE in the PBS of pH 7.4 before (a) and after incubated in the H1 solution containing 10.0 fM ctDNA (b) and MCH/MB-P1/Fc-P2/U–Au-MGA/GCE in the PBS of pH 7.4 before (c) and after incubated in the H1 solution containing 10.0 fM ctDNA (d) and the corresponding relationship curves of the logarithm of I_{MB}/I_{Fc} value with the logarithm of ctDNA concentration.

detection of ctDNA (kras mutation), several DNA species were designed to simulate main interferences, including blank group, mutant gene sequences, wild type sequences and random sequences. Fig. s2 shows that the blank control group, wild type and random sequence only cause a minor change in the DPV peak current of MB and Fc as well as the I_{MB}/I_{fc} values, which fluctuate slightly compared to the blank control group. Correspondingly, target mutant gene kras (G12A) causes the lowest I_{Fc} and highest I_{MB}. Its the I_{MB}/I_{fc} value is much higher than that caused by the interference source signal, indicating that the as-proposed biosensor has good specificity for ctDNA. Therefore, the as-proposed biosensor can effectively detect mutated genes in clinical samples.

3.6. Sample analysis

The proposed biosensor was used to detect of the ctDNA of the KRAS gene associated with colorectal cancer in diluted serum samples. Recovery experiments were carried out by adding target DNA of known concentration into blood samples of healthy volunteers. Table 3 shows that the recovery rate is in the range of 95.8–104.8%, which proves that the biosensor has excellent precision and accuracy. In addition, we also used ctDNA isolated from patients with Kras mutation-positive lung cancer to verify the practicality of the constructed electrochemical sensor. The results showed that the results of proposed method are consistent with those obtained by the fluorescence-based method, sufficiently

Table 3
The results for electrochemical detection of ctDNA gene fragments in the PCR products from human blood (N = 5).

Samples	Targent DNA added (fM)	KRAS (G12A) gene ragments found by the proposed method (fM)	KRAS (G12A) gene ragments found by the fluorescence-based method (fM) [35]	Recovery (%)
Human blood of healthy volunteer 1#	0.0	No found		95.8
	5.0	4.79 ± 0.32		
Human blood of healthy volunteer 2#	0.0	No found		102.2
	10.0	10.22 ± 0.64		
Human blood of healthy volunteer 3#	0.0	No found		104.8
	50.0	52.4 ± 0.88		
Human blood of cancer patient 1#	0.0	5.72 ± 0.43	5.66 ± 0.54	
Human blood of cancer patient 2#	0.0	14.86 ± 0.75	13.1 ± 0.91	
Human blood of cancer patient 3#	0.0	12.48 ± 1.62	10.75 ± 2.83	

demonstrating that the proportional electrochemical biosensor has a useful value in identifying ctDNA, a clinical isolate product.

4. Conclusions

This study has demonstrated the sphape-controlled synthesis of gold nanocrystals via the reduction of $HAuCl_4$ with ascorbic acid in the presence of CTAC, KBr, KI and L-glutathione. Due to a significant synergy of shape induction of CTAC, KBr and KI and enantioselective induced growth of L-glutathione, the as-synthesized gold nanocrystals display an urchin-like gold nanostructure with multilevel spikes and more exposed high-index facets. The unique structure achieves to an excellent catalytic activity. The integration of gold nanocrystals and multiple graphene aerogel was used for the construction of electrochemical sensing platform for the detection of circulating tumor DNA coupled with the target DNA-induced recycling amplification. The analytical method provides ultrahigh sensitivity, specificity and repeatability for detection of circulating tumor DNA in human blood.

Declaration of competing interest

The authors declare that they have no known competing financial interests or personal relationships that could have appeared to influence the work reported in this paper.

CRediT authorship contribution statement

Peng Yuanfeng: Visualization, Investigation. **Li Ruiyi:** Investigation. **Sun Xiulan:** Visualization, Investigation. **Wang Guangli:** Validation, Writing - review & editing. **Li Zaijun:** Conceptualization, Methodology.

Acknowledgements

The authors acknowledge the financial support from National Key Research and Development Program of China (No.2018YFC1603001), Emergency response to COVID-19 washing products of Key Laboratory of Synthetic and Biological Colloids, Ministry of Education (No. YJ2020-02), Science Foundation of Jiangsu Province Special Equipment Safety Supervision Inspection Institute (KJ(Y) 2017014), National Natural Science Foundation of China (No.21576115), and MOE & SAFEA for the 111 Project (B13025).

Appendix A. Supplementary data

Supplementary data to this article can be found online at https://doi.org/10.1016/j.aca.2020.04.077.

References

[1] X.Y. Li, M.S. Ye, W.Y. Zhang, D. Tan, N. Jaffrezic-Renault, X. Yang, Z.Z. Guo, Liquid biopsy of circulating tumor DNA and biosensor applications, Biosens. Bioelectron. 126 (2019) 596–607.
[2] R. Atun, F. Cavalli, The global fight against cancer: challenges and opportunities, Lancet 391 (2018) 412–413.
[3] K.M. Koldby, M.B. Mortensen, S. Detlefsen, P. Pfeiffer, M. Thomassen, T.A. Kruse, Tumor-specific genetic aberrations in cell-free DNA of gastro-esophageal cancer patients, J. Gastroenterol. 54 (2019) 108–121.
[4] L. Gorgannezhad, M. Umer, M.N. Islam, N.-T. Nguyen, M.J.A. Shiddiky, Circulating tumor DNA and liquid biopsy: opportunities, challenges, and recent advances in detection technologies, Lab Chip 18 (2018) 1174–1196.
[5] N. Brychta, T. Krahn, O. von Ahsen, Detection of KRAS mutations in circulating tumor DNA by digital PCR in early stages of pancreatic cancer, Clin. Chem. 62 (2016) 1482–1491.
[6] P. Hu, S. Zhang, T. Wu, D. Ni, W. Fan, Y. Zhu, R. Qian, J.L. Shi, Fe–Au Nanoparticle-coupling for ultrasensitive detections of circulating tumor DNA, Adv. Mater. 30 (2018) 1801690.
[7] Q. Zhou, J. Zheng, Z. Qing, M. Zheng, J. Yang, S. Yang, et al., Detection of circulating tumor DNA in human blood via DNA-mediated surface-enhanced Raman spectroscopy of single-walled carbon nanotubes, Anal. Chem. 88 (2016) 4759–4765.
[8] A.H. Nguyen, S.J. Sim, Nanoplasmonic biosensor: detection and amplification of dual bio-signatures of circulating tumor DNA, Biosens. Bioelectron. 67 (2015) 443–449.
[9] J. Das, I. Ivanov, E.H. Sargent, S.O. Kelley, DNA clutch probes for circulating tumor DNA analysis, J. Am. Chem. Soc. 138 (2016) 11009–11016.
[10] F.E. Dewey, S. Pan, M.T. Wheeler, S.R. Quake, E.A. Ashley, DNA sequencing clinical applications of new DNA sequencing technologies, Circulation 125 (2012) 931–944.
[11] Z. Wang, E.S. Xu, C.C. Wang, W. Wei, Y. Liu, S.Q. Liu, High specificity and efficiency electrochemical detection of poly(ADP-ribose) polymerase-1 activity based on versatile peptide-templated copper nanoparticles and detection array, Anal. Chim. Acta 1091 (2019) 95–102.
[12] X. Liu, M. Wei, E.S. Xu, H.T. Yang, W. Wei, Y.J. Zhang, S.Q. Liu, A sensitive, label-free electrochemical detection of telomerase activity without modification or immobilization, Biosens. Bioelectron. 91 (2017) 347–353.
[13] Y.F. Wu, S.Q. Liu, L. He, Polymerization-assisted signal amplification for electrochemical detection of biomarkers, Analyst 136 (2011) 2558–2563.
[14] M. Daneshpour, L.S. moradi, P. Izadi, K. Omidfar, Femtomolar level detection of RASSF1A tumor suppressor gene methylation by electrochemical nanogenosensor based on Fe_3O_4/TMC/Au nanocomposite and Pt-modified electrode, Biosens. Bioelectron. 77 (2016) 1095–1103.
[15] D. Li, Y. Xu, L. Fan, B. Shen, X. Ding, R. Yuan, X.M. Li, W.X. Chem, Target-driven rolling walker based electrochemical biosensor for ultrasensitive detection of circulating tumor DNA using doxorubicin@ tetrahedron-Au tags, Biosens. Bioelectron. 148 (2020) 111826.
[16] B. Esteban-Fernández de Ávila, E. Araque, S. Campuzano, M. Pedrero, B. Dalkiran, R. Barderas, R. Villalonga, E. Kiliç, J.M. pingarrón, Dual functional graphene derivative-based electrochemical platforms for detection of the TP53 gene with single nucleotide polymorphism selectivity in biological samples, Anal. Chem. 87 (2015) 2290–2298.
[17] W. Wang, X. Fan, S. Xu, J.J. Davis, X. Luo, Low fouling label-free DNA sensor based on polyethylene glycols decorated with gold nanoparticles for the detection of breast cancer biomarkers, Biosens. Bioelectron. 71 (2015) 51–56.
[18] C. Cai, Z. Guo, Y. Cao, W. Zhang, Y. Chen, A dual biomarker detection platform for quantitating circulating tumor DNA (ctDNA), Nanotheranostics 2 (2018) 12–20.
[19] Y.Y. Ma, Q. Kuang, Z.Y. Jiang, Z.X. Xie, R.B. Huang, L.S. Zheng, Synthesis of trisoctahedral gold nanocrystals with exposed high-index facets by a facile chemical method, Angew. Chem. Int. Ed. 47 (2008) 8901–8904.
[20] Q. Zhang, B. Zang, S. Wang, Surfactant-free synthesis of porous Au by a urea complex, RSC Adv. 9 (2019) 23081–23085.
[21] Z. Liu, Z. Yang, B. Peng, C. Cao, C. Zhang, H. You, Q.H. Xiong, Z.Y. Li, J.X. Fang, Highly sensitive, uniform, and reproducible surface-enhanced Raman spectroscopy from hollow Au-Ag alloy nanourchins, Adv. Mater. 26 (2014) 2431–2439.
[22] R.Y. Li, L. Liu, H.Y. Zhu, Z.J. Li, Synthesis of gold-palladium nanowaxberries/dodecylamine-functionalized graphene quantum dots-graphene micro-aerogel for voltammetric determination of peanut allergen Ara h 1, Anal. Chim. Acta 1008 (2018) 38–47.
[23] S. Sen, S. Dasgupta, S. DasGupta, Does surface chirality of gold nanoparticles affect fibrillation of HSA? J. Phys. Chem. C 121 (2017) 18935–18946.
[24] G. Darabdhara, M.R. Das, S.P. Singh, A.K. Rengan, S. Szunerits, R. Boukherroub, Ag and Au nanoparticles/reduced graphene oxide composite materials: synthesis and application in diagnostics and therapeutics, Adv. Colloid Interface Sci. 271 (2019) 101991.
[25] R.Y. Li, L. Liu, H.X. Bei, Z.J. Li, Nitrogen-doped multiple graphene aerogel/gold nanostar as the electrochemical sensing platform for ultrasensitive detection of circulating free DNA in human serum, Biosens. Bioelectron. 79 (2016) 457–466.
[26] C. Barbero, J. Silber, L. Sereno, Studies of surface-modified glassy carbon electrodes obtained by electrochemical treatment: its effect on $Ru(bpy)_3^{2+}$ adsorption and the electron transfer rates of the Fe^{2+}/Fe^{3+} couple, J. Electroanal. Chem. 248 (1998) 321–340.
[27] M. Wang, T. Odoom-Wubah, H.M. Chen, X.L. Jing, T. Kong, D.H. Sun, J.L. Huang, Q.B. Li, Microorganism-mediated synthesis of chemically difficult-to-synthesize Au nanohorns with excellent optical properties in the presence of hexadecyltrimethylammonium chloride, Nanoscale 5 (2013) 6599–6606.
[28] Hsin-Lun Wu, Chun-Hong Kuo, Michael H. Huang, Seed-mediated synthesis of gold nanocrystals with systematic shape evolution from cubic to trisoctahedral and rhombic dodecahedral structures, Langmuir 26 (2010) 12307–12313.
[29] D.V.R. Kumar, A.A. Kulkarni, B.L.V. Prasad, Synthesis of triangular gold nanoplates: role of bromide ion and temperature, Colloids Surf., A 422 (2013) 181–190.
[30] M.J. Sun, G.J. Ran, Q. Fu, W.L. Xu, The effect of iodide on the synthesis of gold nanoprisms, J. Exp. Nanosci. 10 (2015) 1309–1318.
[31] J. Luo, Y. Cheng, Z.-W. Gong, K. Wu, Y. Zhou, H.X. Chen, M. Gauthier, Y.Z. Cheng, J. Liang, T. Zou, Self-assembled peptide functionalized gold nanopolyhedrons with excellent chiral optical properties, Langmuir 36 (2020) 600–608.
[32] L.D. Li, Y. Peng, Y.H. Yue, Y. Hu, X. Liang, P.G. Yin, L. Guo, Synthesis of concave

gold nanocuboids with high-index facets and their enhanced catalytic activity, Chem. Commun. 51 (2015) 11591–11594.
[33] X. Chen, Y. Tang, R. Yan, P. Miao, Ultrasensitive detection of ctDNA by target-mediated in situ growth of dna three-way junction on the electrode, ChemElectroChem 7 (2020) 64–68.
[34] B. Qiu, L. Guo, C. Guo, Z. Guo, Z. Lin, G. Chen, Synthesis of a new Ni-phenanthroline complex and its application as an electrochemical probe for detection of nucleic acid, Biosens. Bioelectron. 26 (2011) 2270–2274.
[35] Eugene J.H. Wee, Y.L. Wang, S.C.H. Tsao, M. Trau, Simple, sensitive and accurate multiplex detection of clinically important melanoma DNA mutations in circulating tumour dna with SERS nanotags, Theranostics 6 (2016) 1506–1513.